Topological surface states in the Kondo insulator YbB_{12} revealed via planar tunneling spectroscopy

A. Gupta,[1,2] A. Weiser,[3] L. Pressley,[4,*] Y. Luo,[4] C. Lygouras,[4] J. Trowbridge,[5] W. A. Phelan,[4,5,6,†] C. L. Broholm,[4] T. M. McQueen,[4,5,7] and W. K. Park[1,‡]

[1]*National High Magnetic Field Laboratory, Florida State University, Tallahassee, Florida 32310, USA*

[2]*Department of Physics, Florida State University, Tallahassee, Florida 32306, USA*

[3]*Department of Physics, Astronomy, Geology, and Environmental Science, Youngstown State University, Youngstown, Ohio 44555, USA*

[4]*Institute for Quantum Matter and William H. Miller III Department of Physics and Astronomy, Johns Hopkins University, Baltimore, Maryland 21218, USA*

[5]*Department of Chemistry, Johns Hopkins University, Baltimore, Maryland 21218, USA*

[6]*Hopkins Extreme Materials Institute, Johns Hopkins University, Baltimore, Maryland 21218, USA*

[7]*Department of Materials Science and Engineering, Johns Hopkins University, Baltimore, Maryland 21218, USA*

(Received 6 December 2022; revised 22 March 2023; accepted 22 March 2023; published 18 April 2023)

Planar tunneling spectroscopy of the Kondo insulator SmB_6 suggests that an interaction between the surface Dirac fermions and the bulk spin excitons results in incompletely protected topological surface states. To gain further insight into their true nature, it is necessary to study other topological Kondo insulator candidates. Calculations of electronic energy bands predict that the Kondo insulator YbB_{12} hosts topological surface states protected by crystalline mirror symmetry. In this study, we present tunneling conductance spectra obtained from the (001) surface of YbB_{12} single crystals and discuss them in comparison to SmB_6. The linear conductance at low bias provides strong evidence for the existence of surface Dirac fermions. The double-hump structure in the negative-bias region is associated with hybridized band edges, in agreement with a calculated band structure. While these similarities with SmB_6 are suggestive of the existence of topological surface states in YbB_{12}, in agreement with other experiments, some discrepancies are also observed, which we attribute to a difference in their exact nature from those in SmB_6.

DOI: 10.1103/PhysRevB.107.165132

I. INTRODUCTION

The remarkable discovery that band insulators can be classified into topologically distinct classes by virtue of their topological indices gave birth to the exciting field of topological insulators (TIs) [1,2]. The transition from a topologically trivial to a nontrivial phase of the same insulator is not associated with the breaking of any symmetry and thus cannot be understood within the Ginzburg-Landau picture [3]. Such a topological phase transition can only occur by closing and reopening the band gap, which gives rise to conducting surface states (SS) protected by spin-momentum locking [4]. The nature of these SS heavily depends on the strength of the electron correlations in each material. Therefore, the SS in weakly correlated *s*- and *p*-orbital systems like HgTe [5–7] and the Bi_2Se_3 family of compounds [8–10] are less complex to understand than those in *d*- and *f*-orbital systems because of the added ingredient of strong correlations [11]. Kondo insulators (KIs) are one such class of strongly correlated materials, in which the hybridization between the conduction band and the localized states results in the opening of a hybridization gap around the Fermi level at low temperature [12,13]. The hybridized band edges are brought closer due to the strong correlation effect, resulting in a reduced gap [12,14]. In combination with the large spin-orbit interaction, this can cause band inversions in these compounds. Due to the odd parity of f states, band inversions at odd number of high-symmetry points can give rise to a topologically nontrivial phase, known as topological Kondo insulators (TKIs) [14].

In the KI SmB_6, such a hybridization takes place between the $4f$ orbitals and $5d$ bands, resulting in a nontrivial Z_2 topological phase protected by time-reversal symmetry [1,2] and hence making it a prime TKI candidate [11,15]. This theoretical prediction has stimulated extensive studies of SmB_6. The low-temperature resistance plateau, which was repeatedly observed in various transport measurements, has been attributed to the topologically protected SS [16–18]. While the observation of de Haas–van Alphen (dHvA) effect in SmB_6 suggests the presence of Fermi surfaces in SmB_6 [19–22], the absence of Shubnikov–de Haas (SdH) oscillations remains a mystery. Furthermore, the exact origin of the dHvA oscillations in SmB_6 is still under debate [19–22]. The hybridization gap has been detected in photoemission [23–29], tunneling [30–34], and point-contact spectroscopic [35] studies. Our recent planar tunneling spectroscopy (PTS) studies on SmB_6 have provided clear signatures for surface Dirac fermions [33], in good agreement with electronic energy band calculations

*Present address: Oak Ridge National Laboratory, Oak Ridge, TN 37830, USA.

†Present address: Los Alamos National Laboratory, Los Alamos, Mail Stop E574, Los Alamos, NM 87545, USA.

‡wkpark@magnet.fsu.edu

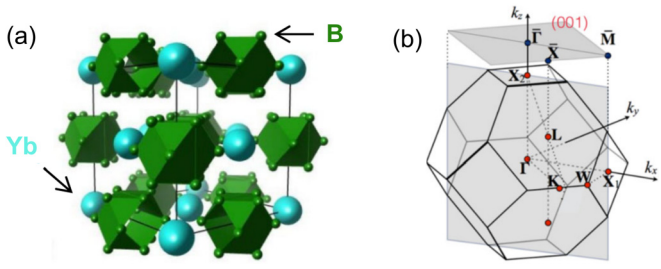

FIG. 1. (a) Crystal structure of KI YbB_{12} (adapted from Ref. [36]). YbB_{12} has a face-centered cubic (fcc) structure similar to NaCl. The Yb ions (cyan spheres) make up the fcc lattice like Na and the B_{12} cubo-octahedra (green) take up the Cl positions. (b) Bulk and (001) surface Brillouin zones of YbB_{12} (adapted from Ref. [47]). The (001) surface has been studied by PTS in this study.

[14,37–39] and a quantum oscillation study [19]. Moreover, the topological surface states (TSS) were found to interact with the bulk spin excitons [40], a precursor excitation occurring near an antiferromagnetic quantum critical point [41], in agreement with a theoretical prediction [41] and an angle-resolved photoemission spectroscopy (ARPES) study [42]. Such an interaction would result in incomplete protection of the TSS. Even though the helical spin texture of the SS of SmB_6 was reported in some measurements [29,43,44], it still requires further investigations particularly considering that the topological nature of the SmB_6 SS has been debated [15,45]. This motivates us to study another TKI candidate to better understand the origin of the metallic SS in these materials.

Ytterbium dodecaboride (YbB_{12}) is another prototypical KI, which has a face-centered cubic structure with the lattice constant of 7.468 Å [Fig. 1(a)], much larger than that of SmB_6 (4.134 Å) [46]. The calculated band structure of YbB_{12} differs from SmB_6 in that the band inversion occurs twice at each of the three X points [Fig. 1(b)] [47], resulting in a trivial Z_2 invariant. Instead, band calculations for the (001) surface [47] show that YbB_{12} is a topological crystalline insulator [48,49] with a nontrivial mirror Chern number protected by crystalline reflection symmetry with respect to the $\Gamma X_1 X_2$ mirror plane. Transport measurements on YbB_{12} single crystals reveal two activation-type energy gaps, 11.7 meV (below 40 K) and 3.8 meV (below 15 K) [50], but their origin is yet to be understood. YbB_{12} shows a low-temperature resistivity plateau similar to SmB_6, which can be attributed to the TSS. The weak antilocalization effect displayed in the magnetoresistance of YbB_{12} microstructures has been argued to arise from the spin-momentum locking property of the surface states [50]. Measurements of the heat capacity and thermal conductivity have revealed finite linear temperature-dependent terms in the zero-temperature limit, suggesting the existence of gapless charge-neutral fermions [51]. The formation of the hybridization gap was observed in optical conductivity [52] and photoemission spectroscopy measurements [53,54]. The optical conductivity measurements found the size of the indirect (direct) gap to be 15 meV (∼180 meV) [52]. Studies based on inelastic neutron scattering have found in-gap spin excitations at two energy scales, 14.5 meV and 20 meV [55], but a Lu-substitution study has suggested that a more local phenomenon is responsible for the formation of the gap [56]. The hybridization gap can be closed at high magnetic fields in the range of 45–47 T ($H \parallel [100]$) and 55–59 T ($H \parallel [110]$), turning the system into a metallic state [57–61]. Quantum oscillations have been observed in YbB_{12} arising from the dHvA and SdH effects in the metallic regime [61,62] as well as in the insulating phase [50,60,62–64]. The angular variation of the SdH period was found to point to a three-dimensional Fermi surface [63] but such oscillations were not observed in microstructured YbB_{12} single crystals [50], both of which indicate that these oscillations originate from the electrically insulating bulk. This is rather puzzling since the insulating bulk is not expected to contain a Fermi surface. On the other hand, the origin of the dHvA oscillations in YbB_{12} is under debate [60,63].

However, transport measurements alone are not enough to elucidate the topological nature of the SS of a KI and direct investigations of the SS in YbB_{12} have not been done extensively. An ARPES study on a clean (001) surface of this material revealed surface-band dispersion consistent with what is expected from the SS of a TKI [65] but could not establish the existence of TSS with absolute certainty. The spin texture in the SS of YbB_{12} also remains to be determined.

In this work, we report a PTS study on the (001) surface of the single-crystalline KI YbB_{12}, in which we discuss our findings in comparison to the results from recent transport measurements [50] and the ARPES study [65]. We also compare YbB_{12} against the better understood KI SmB_6 to see if the interaction between the bulk excitations and the surface states [33] exists similarly in the two. In our PTS study, YbB_{12} exhibits linear conductance at low bias, a signature originating from the V-shaped Dirac fermion density of states (DOS) around the Dirac point. The overall shape is similar to SmB_6 except that the bias voltage at which the linearity ends is much lower than the hybridization gap edges. Additionally, the conductance curves when Pb is superconducting do not show any additional pronounced peak. Such a peak at 5 mV signified inelastic tunneling involving bulk excitons in SmB_6 [33]. Based on these signatures and other details, we discuss the topological nature of the surface states in the KI YbB_{12}.

II. MATERIALS AND METHODS

The YbB_{12} single crystals used in this study were grown by the traveling solvent floating-zone method [66]. The orientation of as-grown crystals was determined using the backscattered x-ray Laue diffraction technique and then they were cut along the (001) direction into rectangular parallelepiped shape. Three of such cut pieces were used for the experiments in this study. The dc resistance of the unpolished and polished crystals was measured using the standard four-probe method by attaching thin aluminum strips using silver paint.

A similar procedure for making tunnel junctions on single crystals of YbB_{12} was followed as had been used for SmB_6 single crystals [33]. Each cut piece was embedded in a mold made of Stycast® epoxy (2850-FT) and then polished. Tunnel junctions were made repeatedly on the three crystals by repolishing them after each measurement was completed. Surface smoothness on the atomic scale, essential for high-quality tunnel junctions, is achieved by polishing with diamond lapping

films in the range of 3–0.25 μm particle size. Atomic force microscopy of the polished surfaces reveals a peak-to-dip roughness less than 10 Å (see Supplemental Material [67]), showing that smooth and clean crystal surfaces are achieved after polishing. These polished crystals are etched with an argon ion beam in a high-vacuum chamber to remove any contaminants on the surface and to obtain a boron-rich top layer, which is then plasma oxidized in the same chamber to form boron oxide to serve as the tunnel barrier [68]. Since the characteristics of the tunnel barrier are extremely sensitive to both ion beam etching and plasma oxidation processes, the etching/oxidation power and durations were optimized through multiple runs. The crystal edges are then painted with Duco® cement to ensure the electrical isolation on the edges and to define the junction areas, after which the counter electrode is deposited by thermal evaporation. Typical junction dimensions are in the range of $(0.2-0.3) \times (0.1-0.7)\,\mathrm{mm}^2$. For the measurement of the differential conductance, thin aluminum strips are attached to both the bottom and top electrodes. The measurement is done by a standard four-probe lock-in technique as a function of temperature down to 1.75 K and magnetic field up to 14 T.

III. RESULTS AND DISCUSSION

The temperature dependence of the dc electrical resistance, $R(T)$, is measured across the (001) surface of one of the YbB_{12} crystals used in our PTS study and normalized against its resistance at room temperature, $R_N(T)$ as shown Fig. 2(a). In order to see whether the crystal shows similar temperature dependence before and after the polishing process, the normalized dc resistance at both stages of the crystal is compared. The temperature dependence remains almost the same, attesting the robustness of the surface states against a harsh process like that of polishing, as is the case for SmB_6 [33]. The inset of Fig. 2(a) shows the $R(T)$ for all the three crystals, indicating that it is similar in all the crystals including the increase by about five orders of magnitude, a typical insulating behavior. A closer inspection reveals that this increase in $R(T)$ is not monotonic, suggesting that YbB_{12} is not a trivial bulk insulator. More specifically, the slope of the $R(T)$ curve increases below ∼50 K, similar to SmB_6 [33]. This increase in the slope of the $R(T)$ curve indicates more insulating character and therefore, this can be attributed to the hybridization gap opening in the bulk. This is followed by a broad hump in the range of 10–30 K, reminiscent of a similar hump observed in SmB_6 from 15–20 K [33]. A further increase in the slope is observed as the temperature is decreased below 15 K, showing a two-gap behavior. The magnitude of the two gaps is obtained [Fig. 2(b)] by the thermal activation model of resistivity ($\rho \propto e^{\Delta/2kT}$, where ρ = resistivity, Δ = energy gap, k = Boltzmann constant, and T = temperature) and the gap values are found to be $\Delta_1 = 10.95$ meV ($15\,\mathrm{K} < T < 40\,\mathrm{K}$) and $\Delta_2 = 5.11$ meV ($7\,\mathrm{K} < T < 15\,\mathrm{K}$). While Δ_1 is similar to those obtained in previous transport measurements, Δ_2 is slightly larger ($\Delta_1 =$ 10.9–11.2 meV and $\Delta_2 =$ 3.33–4.23 meV, for the same temperature ranges [50]). The Δ_1 value in YbB_{12} is comparable to SmB_6 ($\Delta_1 =$ 10.4–11.2 meV), whereas Δ_2 is bit larger in SmB_6 ($\Delta_2 =$ 5.8–6.6 meV) [69].

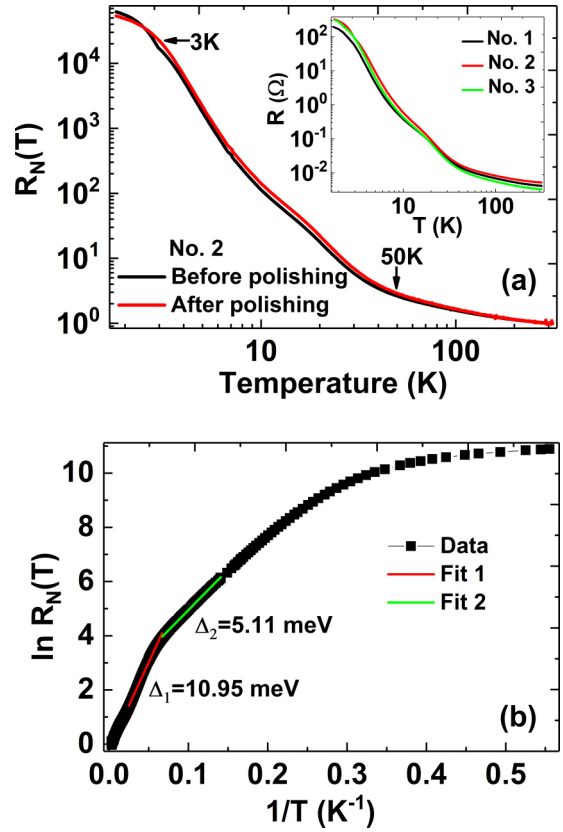

FIG. 2. (a) dc resistance normalized against room temperature resistance before and after polishing the crystal. (Inset) Resistance of all the three YbB_{12} crystals. Change in slope at around 50 K and the plateauing below 3 K are marked by arrows. (b) Arrhenius plot of the resistance in (a). The linear fit of the low temperature data shows a two-gap behavior: $\Delta_1 = 10.95$ meV ($15\,\mathrm{K} < T < 40\,\mathrm{K}$) and $\Delta_2 =$ 5.11 meV ($7\,\mathrm{K} < T < 15\,\mathrm{K}$).

According to the theory [14], the metallic SS are expected to develop in close correspondence with the formation of the bulk gap in KIs. But experimentally, the opening of this bulk hybridization gap in SmB_6 is not immediately accompanied by the development of the conducting SS. This was speculated to be due to the interaction between the SS and the bulk spin excitons, which becomes negligible only at a lower temperature where the spin excitons condense [33,69]. The first signatures of the conducting SS only appear when the crystals are further cooled down to about 3–4 K, where there is a rapid decrease in the slope of the $R(T)$ curves [50] indicating the development of the conducting SS. While stoichiometric SmB_6 crystals exhibit a pronounced plateau below ∼4 K [16–18,33], Sm-deficient crystals only show a decrease in the slope but no pronounced plateau down to the lowest measurement temperature [69]. In the present study, the YbB_{12} crystals show a clear decrease in the slope at low temperature (∼3 K), as seen in Fig. 2(a) (A plateau becomes more apparent upon further cooling [67]). Similar to SmB_6, this temperature is much lower than the bulk gap opening temperature and therefore this indicates the presence of interactions between the SS and the bulk spin excitons, as was speculated in the case of SmB_6 [33]. But, transport measurements alone cannot

confirm whether the plateau seen in our resistance data is due to the contribution from the TSS or in-gap states in the bulk arising from disorder. Spectroscopic measurements can help us better address these questions. We have employed PTS since it is a surface-sensitive technique with high energy resolution and momentum selectivity and, thus, well suited for the study of the SS.

We have chosen Pb as the counterelectrode in our tunnel junctions because the sharpness of its superconducting features in the differential conductance, $G(V) = dI/dV$, serves as an important diagnostic for their quality. Figure 3(a) shows the normalized conductance, $G_N(V)$, obtained by dividing $G(V)$ by the value at the negative maximum bias, for two junctions on the same crystal. The sharp Pb superconducting features, i.e., the pronounced coherence peaks and the normalized zero-bias conductance (ZBC) being close to zero ($\sim 6.3 \times 10^{-3}$), confirm their high quality. Both conductance curves are similar in their overall shape. However, they are different in some detailed features including the sharpness of coherence peaks and the depths of the ZBC, which can be due to a slight difference in the microstructure of the junction area. Figure 3(b) compares the sharpness of the Pb superconducting features observed in different junctions prepared with different parameters for the ion beam etching and plasma oxidation. Similar sensitiveness of the junction quality to such processing parameters was also reported for SmB_6 [68], wherein it was speculated that the layer of disrupted boron octahedra resulting from the ion beam etching process might be too thin if the ion beam energy is low or it becomes inhomogeneous if the ion beam energy is high. The asymmetry of the coherence peaks is highly reproducible across junctions irrespective of the details of the barrier formation, which originates from the intrinsic DOS of the YbB_{12}, as seen below. Amongst the two junctions in Fig. 3(a) which show the lowest ZBC, the junction labeled as J1 is of higher quality as evidenced by more prominent coherence peaks. Plotted in Fig. 3(c) is the conductance taken after Pb is driven normal by an applied magnetic field. Further increasing the field well above the Pb critical field shows no change at low bias, but a slight increase at higher bias, whose origin is not currently clear [67].

Another standard diagnostic for the quality of the tunnel barrier is fitting the $G(V)$ data in the high-bias region, which may contain only the barrier effect, to the Brinkman-Dynes-Rowell (BDR) model [70]. According to this model, such background conductance exhibits quadratic dependence on the bias voltage as follows:

$$G(V) = 3.16 \times 10^{10} H^{1/2} d e^{-1.025 d H^{1/2}} \times [1 - 0.171\, d\Gamma H^{-3/2} V + 0.525 d^2 H^{-1} V^2], \quad (1)$$

where d is the barrier thickness (in Å), H is the barrier height (in eV), and Γ is the asymmetry of the barrier (in eV). As shown in Fig. 4, the fitting for J1 is good, giving reasonable values for the fitting parameters: $d = 18.49$ Å, $H = 3.25$ eV, and $\Gamma = 1.19$ eV. This indicates that the tunnel barrier formed with optimized processing parameters for the ion beam etching and plasma oxidation is of a desirable shape. On the other hand, changing the processing parameters slightly results in a poor tunnel barrier (S2) with very different fitting parameters ($d = 24.85$ Å, $H = 2.02$ eV, and $\Gamma = 3.13$ eV) in which the barrier height is less than the barrier asymmetry. This further attests the high sensitivity of the barrier properties to the processing parameters [68].

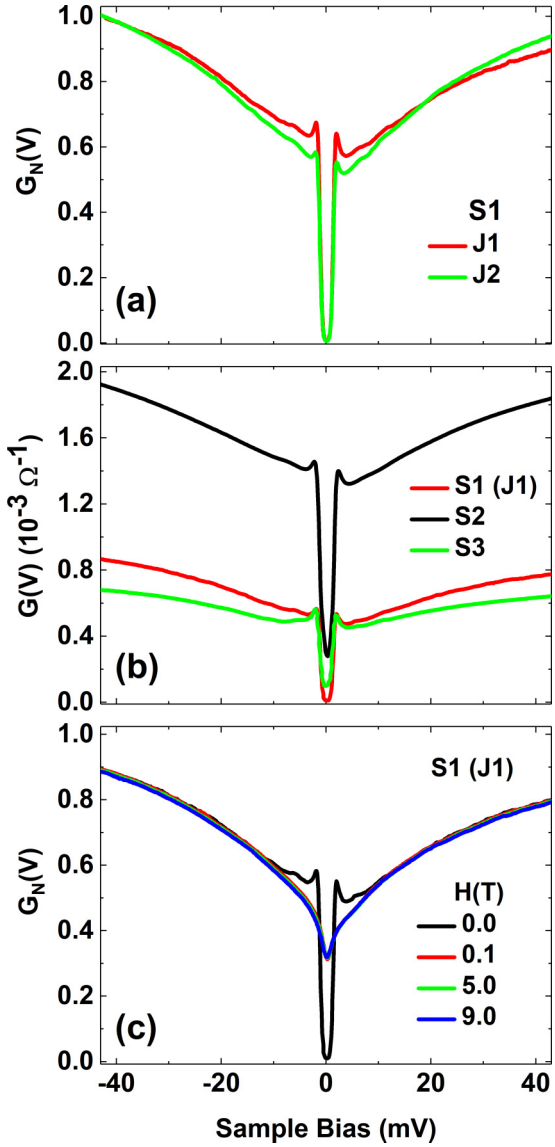

FIG. 3. (a) Normalized $G(V)$ for two representative high-quality junctions with Pb as counterelectrode taken at $T = 1.75$ K and $H = 0$ G. (b) Comparison of $G(V)$ of junctions on different crystal surfaces processed using different conditions. Quality of the junction is characterized by the sharpness of the coherence peaks and the depth of the zero-bias dip. Key process parameters for the ion beam etching and plasma oxidation used for each junction are shown in the following, in the order of (beam voltage, beam current, etching time, plasma power, oxidation time): S1(J1) = (100 V, 4 mA, 1 min 20 s, 1 W, 1 min); S2 = (100 V, 4 mA, 1 min 40 s, 0.89 W, 0.5 min); S3 = (300 V, 10 mA, 1 min, 1 W, 1 min). (c) Magnetic field dependence of the normalized $G(V)$. There is no change in $G(V)$ as the field is increased above 0.1 T. Below 0.1 T, the superconducting features of Pb are visible.

Normalizing the $G(V)$ when the Pb is in a superconducting state against that obtained when the Pb is driven to a normal state at the same temperature by applying a magnetic field of 0.1 T removes the features intrinsic to YbB_{12}. This

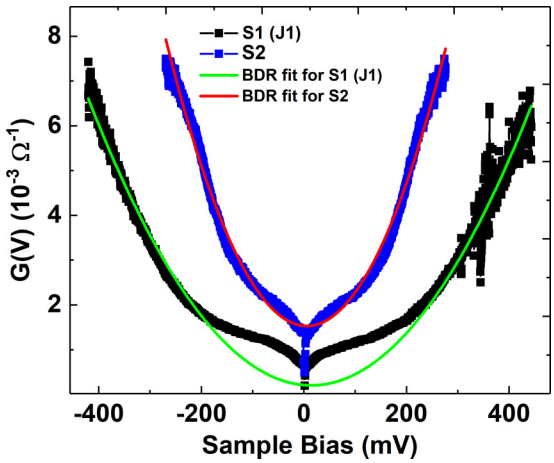

FIG. 4. BDR fit for the high-bias region of the $G(V)$ for two typical junctions. Barrier parameters for J1 are found to be $d = 18.49$ Å, $H = 3.25$ eV, and $\Gamma = 1.19$ eV. These values show that the tunnel barrier has a desirable shape. On the other hand, slightly different processing parameters were used in S2, whose barrier parameters are found to be $d = 24.85$ Å, $H = 2.02$ eV, and $\Gamma = 3.13$ eV. These values indicate poorer barrier quality.

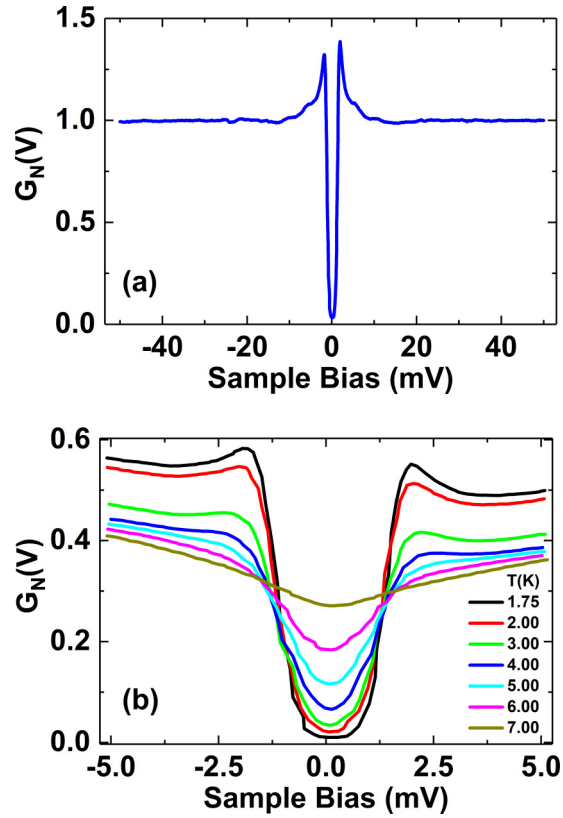

FIG. 5. (a) $G(V)$ with Pb in superconducting state normalized against $G(V)$ with Pb in normal state for junction S1(J1). No obvious features other than the Pb superconducting features are observed. (b) Temperature evolution of the Pb coherence peaks for junction S1(J1). Asymmetry between the coherence peaks stays constant as the temperature is changed. Peaks vanish once the Pb is in a normal state.

helps to study additional attributes in the conductance curves arising from other channels, e.g., involving inelastic tunneling [33,69]. Such a normalized $G(V)$ curve is shown in Fig. 5(a). It does not exhibit any additional features like the peak near +5 mV observed in SmB_6 [33]. This suggests that in this compound the interaction of the bulk spin excitons with the SS is not obvious down to the lowest measurement temperature (1.75 K), unlike in the case of SmB_6. On the other hand, while the asymmetry in the relative height of the coherence peaks in Fig. 5(a) may seem to be pointing towards the presence of such an interaction between the SS and the bulk excitons as in SmB_6 [33], the slight difference from SmB_6 in their temperature evolution raises questions on the origin of this asymmetry. This can be seen from the temperature evolution of the coherence peaks in Fig. 5(b), where the asymmetry between the two peaks remains almost constant till they disappear near the critical temperature ($T_c = 7.25$ K) of Pb. This is unlike SmB_6, where the asymmetry in the relative height of the coherence peaks increases with increasing temperature until they vanish at the T_c of Pb [33]. These features, which are absent in YbB_{12} data, were attributed to the inelastic tunneling involving bulk spin excitons in SmB_6 [33], suggesting that the SS interact with the bulk excitons. Their absence in the present conductance spectra indicates that the topological nature of the SS in YbB_{12} is very different from that of SmB_6 as similar studies on SmB_6 indicate that such interactions between the surface state and the bulk excitons alter the topological protection of the surface state drastically [33,41]. Measuring the conductance at even lower temperatures and the second harmonics may provide further information with regards to the presence of bulk excitations in YbB_{12} and their interactions with its SS.

The V-shaped conductance at low bias, as expected for the Dirac fermion DOS, is clearly seen in Fig. 6(a) when the Pb is driven to a normal state. This linearity starts tapering off slowly outside the ±2 mV range. This is a very narrow region compared to the size of the bulk gap found by other studies (∼15 mV) [52]. As already discussed regarding the temperature dependence of the electrical resistance, this noncorrelation between the emergence of the SS and the bulk hybridization gap, also seen in SmB_6 [33], can be explained by the interaction of the SS with the bulk spin excitons resulting in the incoherence of the SS. In spite of this similarity in the low-bias feature with SmB_6 [33], two major differences can be seen on a closer inspection. First, the kink-hump structure seen in the SmB_6 data [33] is absent in YbB_{12}. While the kink-hump structure in SmB_6 was associated with elastic tunneling involving bulk spin excitons with which the SS interact, the absence of this structure in the YbB_{12} spectra does not rule out such an interaction either, as already suggested by the noncorrelation between the emergence of these SS and the bulk hybridization gap. This indicates that the possible interaction of the SS with bulk spin excitons is manifested very differently in YbB_{12}, possibly due to the difference in the exact topological nature of the YbB_{12} surface from SmB_6. Second, the linear conductance at low bias shows only one slope. This indicates that the YbB_{12} (001) surface has only one kind of Dirac band, unlike in the SmB_6 (001) surface [33]. This is supported by theoretical band calculations [47], which indicate that four Dirac points appear at the four M points on

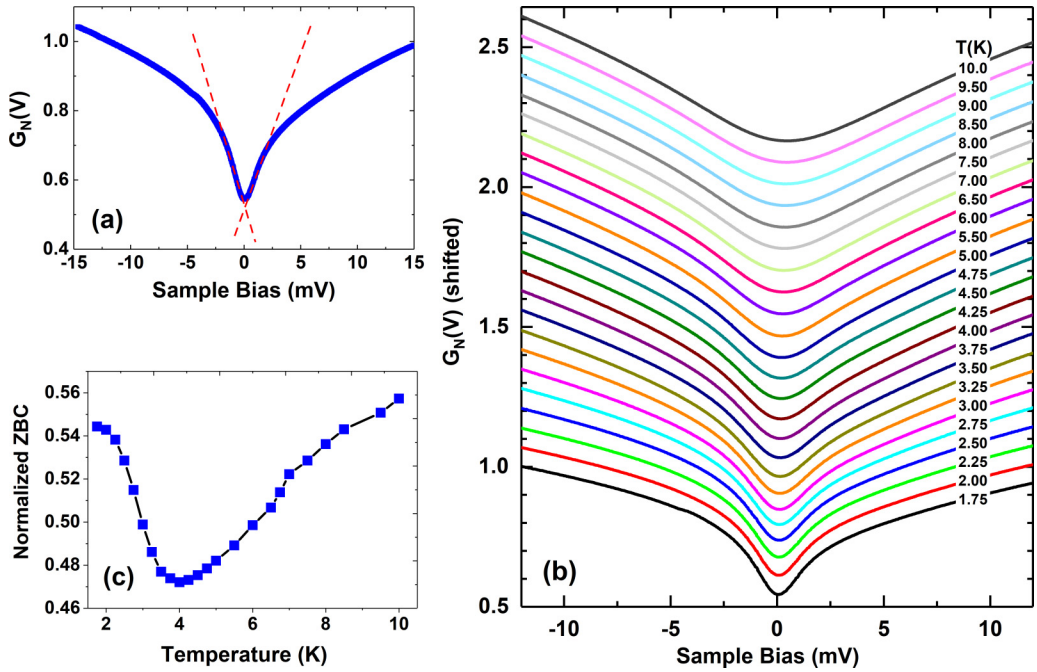

FIG. 6. (a) Normalized $G(V)$ at low bias for junction S2 showing V shape as expected for Dirac fermions. A magnetic field of 0.1 T was applied to drive the Pb to normal state and the temperature was kept constant at 1.75 K. Linearity is similar on both sides of zero bias and tapers off outside the ± 2 mV range. Red dashed lines are drawn as a guide to the eye. (b). Temperature evolution of the normalized $G(V)$ at low bias for junction S2. Curves are shifted vertically for visibility. Linearity gradually becomes less prominent as the temperature is increased, vanishing above 3 K. (c) Normalized ZBC vs T derived from (b). There is a turning point seen at around 4 K due to the emerging surface states. At the lowest measurement temperature of 1.75 K, there is a clear sign of plateauing signifying that the surface state contribution dominates below this temperature.

the (001) surface of YbB_{12} and hence, four Dirac bands of the same type contribute to the low-bias conductance shown in Fig. 6(a). While the qualitative similarity in the low-bias conductance between YbB_{12} and SmB_6 is evidence for the topological origin of the SS in YbB_{12}, in agreement with other experiments [50,65], the minute differences between the two discussed in this section indicate that the SS in these two materials are not exactly the same. Band calculations also indicate that YbB_{12} is a much more strongly correlated insulator than SmB_6 and that YbB_{12} is a topological crystalline insulator, unlike SmB_6 which is a Z_2 topological insulator [47].

The temperature dependence of $G(V)$ in the low-bias region (with the Pb driven normal) is shown in Fig. 6(b). The linearity starts to vanish as the temperature is increased above $\sim$3 K, which agrees with the corresponding change in the resistance slope shown in Fig. 2(a). This further strongly ties the origin of the resistance slope change to the TSS. Also, the $G(V)$ does not show any additional feature, e.g., a peak arising from a trivial origin like an impurity band. The temperature evolution in Fig. 6(b) is used to obtain the normalized ZBC at different temperatures, which is plotted in Fig. 6(c). A turning point can be seen around 4 K, below which these topological surface states can be said to develop and therefore dominantly contribute to the conductance [33,69]. In contrast to SmB_6 [33], the normalized ZBC in YbB_{12} does not exhibit clear plateauing down to the lowest measurement temperature (1.75 K), in line with the resistance behavior seen in our single-crystal samples (Fig. 2). Also, these results are consistent with the literature since the single crystals used in our study fall to the thick limit ($>$100 μm), and thus the SS contribution becomes dominant only at low temperature as reported from a thickness-dependent transport study [50], in which a simple model considering the relative weight between contributions from two parallel conduction channels was adopted to analyze the data. It is an open question whether a similar thickness dependence will be observed in tunneling spectroscopy. In this regard, it is noted that the resistive plateauing occurs below a much lower temperature ($<$20 K) even in the thinnest crystal (0.6 μm) than the hybridization-gap opening temperature (50–100 K). This suggests that there may exist some other factors determining the temperature below which the SS signatures become visible than the relative weight. We argue that the interaction between the SS and the spin excitons could be an important factor as it has been reported in the literature [33,41,42,69].

Figures 7(a) and 7(b) show the temperature evolution of $G(V)$ over a much wider bias range for two junctions prepared on different crystals whose surfaces were processed under slightly different conditions. Figure 7(c) shows the corresponding temperature evolution of the ZBC in these two junctions. While Fig. 7(a) is for a junction with sharp Pb superconducting features, Fig. 7(b) is for a junction with significantly smeared Pb features. At low temperature, both junctions exhibit a characteristic hump structure around -50 mV. Interestingly, it consists of far more pronounced double humps in Fig. 7(b), which is unexpected since this junction shows more smeared Pb coherence peaks than the other junction as mentioned above. As the temperature is

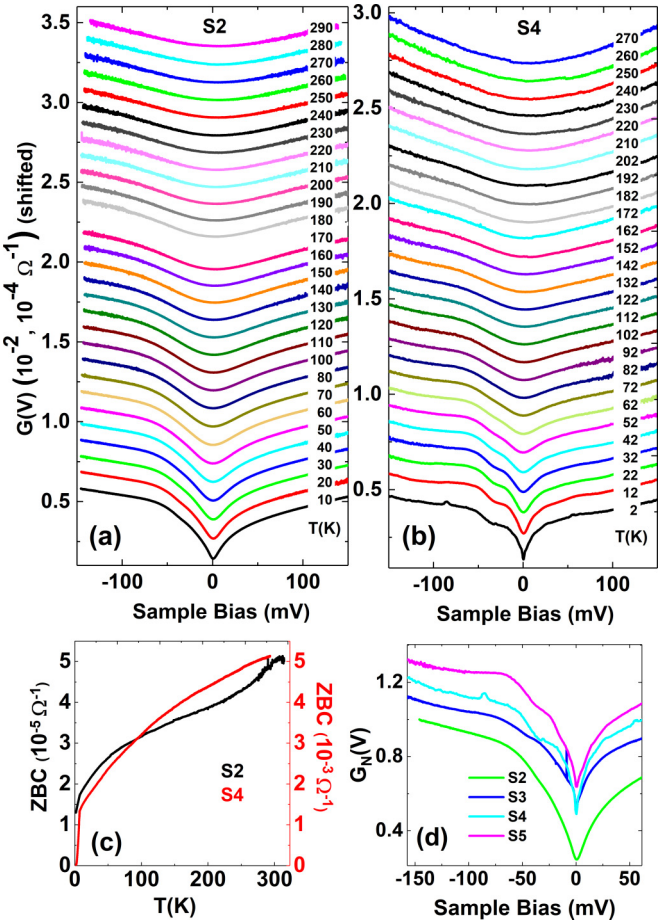

FIG. 7. (a) Temperature dependence of $G(V)$ for junction S2. The double-hump structure around 50 mV is smeared and appears as a single hump. Curves become parabolic above $\sim$ 200 K. (b) Temperature dependence of $G(V)$ for junction S4. The double-hump structure around 50 mV can be clearly seen. As the temperature is increased, the double hump turns into a single hump and then vanishes above $\sim$ 220 K. (c) ZBC vs T for the junctions S2 and S4. ZBC decreases gradually at high temperature, but the slope increases with decreasing temperature beginning at 50–100 K due to the opening of a hybridization gap. Exact origin of the dissimilar onset temperatures is not known. ZBC drops rapidly below the $T_c(= 7.25\,\mathrm{K})$ of Pb due to the opening of a superconducting energy gap. (d) Normalized $G(V)$ curves for various junctions zoomed around the double-hump structure.

increased, this double-hump structure gets thermally smeared, resulting in a single hump, and finally vanishing around 220 K. The curves in Fig. 7(a) also seem to become parabolic above $\sim$200 K. The prominence of the double-hump structure appears uncorrelated with the sharpness of Pb coherence peaks, as seen in all measured junctions [67], but always appear in the negative-bias region and approximately in the same bias voltage range. The double-hump structure across different junctions is compared in Fig. 7(d). Their temperature dependence is also similar across all these junctions, indicating a common origin. A similar double-hump structure in the negative-bias region was also seen in SmB_6 [34] around -25 mV. The band calculations in YbB_{12} show two bands very close to each other near the X point [47] around the same energy range where the double-hump structure is observed in our data. These bands coincide at the Γ point and start separating as the X point is approached. Since in our PTS study the major tunneling direction is [001], that is, along the Γ-X direction [Fig. 1(b)], we speculate that the double-hump structure may originate from these two closely spaced bands near the X point. We further speculate that the variation in its prominence may have to do with the detailed surface microstructure as the prominence is comparable among the junctions in each sample. Further investigations are necessary to better understand it.

IV. SUMMARY

In summary, we have obtained tunneling conductance spectra of the (001) surface of YbB_{12} single crystals and analyzed the data in comparison to SmB_6. Similar to SmB_6, the linear conductance obtained at low bias strongly suggests the existence of surface Dirac fermions. The linearity consists of a single slope pointing towards the existence of just one kind of Dirac band on the (001) surface in agreement with results from previous theoretical calculations. The temperature dependence of the low-bias conductance reveals that the contribution from the SS becomes evident only at very low temperatures ($<$4 K) in agreement with the low-temperature resistance behavior. Another similarity to SmB_6 is the double-hump structure seen in the negative-bias region, which has been explained again by theoretical band calculations.

We observe that the temperature at which the metallic SS start dominantly contributing to the conductance is not coincident with the much higher bulk gap opening temperature ($\sim$50 K). Furthermore, the bias up to which the linearity of the conductance exists ($\pm$2 mV) is very low compared to the bulk gap ($\sim$15 mV), suggesting that the SS might lose the coherence well before reaching the band edges. We speculate that just like in SmB_6, this discrepancy from what is expected theoretically may be caused by a possible interaction between the SS and the bulk spin excitons. However, such an interaction is manifested in YbB_{12} very differently as evidenced by the absence of any clear elastic or inelastic tunneling signatures involving these bulk excitons down to the lowest measurement temperature (1.75 K). This difference from SmB_6 qualitatively suggests that even though the SS in YbB_{12} is of topological origin, its exact nature is different from that of SmB_6. Obtaining conductance spectra at lower temperatures corresponding to the clear plateau in the resistivity will help us better understand the interaction between the SS and the bulk excitons. Further theoretical analysis is also required to arrive at a more comprehensive picture of the topological nature of the SS in YbB_{12}.

Additional data related to the crystal growth are available at Ref. [71].

ACKNOWLEDGMENTS

The work at NHMFL and FSU was supported by Grants No. NSF/DMR-2003405, No. NSF/DMR-1644779, and the State of Florida. The work at JHU was funded by Grant No. DOE/BES EFRC DE-SC0019331, JHU Catalyst Fund, and Grant No. NSF/DMR(PARADIM)-2039380.

[1] M. Z. Hasan and C. L. Kane, Colloquium: Topological insulators, Rev. Mod. Phys. **82**, 3045 (2010).

[2] X. L. Qi and S. C. Zhang, Topological insulators and superconductors, Rev. Mod. Phys. **83**, 1057 (2011).

[3] M. Z. Hasan and J. E. Moore, Three-dimensional topological insulators, Annu. Rev. Condens. Matter Phys. **2**, 55 (2011).

[4] L. Fu, C. L. Kane, and E. J. Mele, Topological Insulators in Three Dimensions, Phys. Rev. Lett. **98**, 106803 (2007).

[5] B. A. Bernevig, T. L. Hughes, and S. C. Zhang, Quantum spin Hall effect and topological phase transition in HgTe quantum wells, Science **314**, 1757 (2006).

[6] M. Konig, S. Wiedmann, C. Brune, A. Roth, H. Buhmann, L. W. Molenkamp, X. L. Qi, and S. C. Zhang, Quantum spin Hall insulator state in HgTe quantum wells, Science **318**, 766 (2007).

[7] X. Dai, T. L. Hughes, X. L. Qi, Z. Fang, and S. C. Zhang, Helical edge and surface states in HgTe quantum wells and bulk insulators, Phys. Rev. B **77**, 125319 (2008).

[8] H. J. Zhang, C. X. Liu, X. L. Qi, X. Dai, Z. Fang, and S. C. Zhang, Topological insulators in Bi_2Se_3, Bi_2Te_3 and Sb_2Te_3 with a single Dirac cone on the surface, Nat. Phys. **5**, 438 (2009).

[9] Y. Xia, D. Qian, D. Hsieh, L. Wray, A. Pal, H. Lin, A. Bansil, D. Grauer, Y. S. Hor, R. J. Cava *et al.*, Observation of a large-gap topological-insulator class with a single Dirac cone on the surface, Nat. Phys. **5**, 398 (2009).

[10] Y. L. Chen, J. G. Analytis, J. H. Chu, Z. K. Liu, S. K. Mo, X. L. Qi, H. J. Zhang, D. H. Lu, X. Dai, Z. Fang *et al.*, Experimental realization of a three-dimensional topological insulator, Bi_2Te_3, Science **325**, 178 (2009).

[11] M. Dzero, J. Xia, V. Galitski, and P. Coleman, Topological Kondo insulators, Annu. Rev. Condens. Matter Phys. **7**, 249 (2016).

[12] H. Tsunetsugu, M. Sigrist, and K. Ueda, The ground-state phase diagram of the one-dimensional Kondo lattice model, Rev. Mod. Phys. **69**, 809 (1997).

[13] P. S. Riseborough, Heavy fermion semiconductors, Adv. Phys. **49**, 257 (2000).

[14] M. Dzero, K. Sun, V. Galitski, and P. Coleman, Topological Kondo Insulators, Phys. Rev. Lett. **104**, 106408 (2010).

[15] J. W. Allen, Foreward for special issue of philosophical magazine on: Topological correlated insulators and SmB_6, Philos. Mag. **96**, 3227 (2016).

[16] D. J. Kim, J. Xia, and Z. Fisk, Topological surface state in the Kondo insulator samarium hexaboride, Nat. Mater. **13**, 466 (2014).

[17] P. Syers, D. Kim, M. S. Fuhrer, and J. Paglione, Tuning Bulk and Surface Conduction in the Proposed Topological Kondo Insulator SmB_6, Phys. Rev. Lett. **114**, 096601 (2015).

[18] Y. S. Eo, S. Wolgast, A. Rakoski, D. Mihaliov, B. Y. Kang, M. S. Song, B. K. Cho, M. C. Hatnean, G. Balakrishnan, Z. Fisk *et al.*, Comprehensive surface magnetotransport study of SmB_6, Phys. Rev. B **101**, 155109 (2020).

[19] G. Li, Z. Xiang, F. Yu, T. Asaba, B. Lawson, P. Cai, C. Tinsman, A. Berkley, S. Wolgast, Y. S. Eo *et al.*, Two-dimensional Fermi surfaces in Kondo insulator SmB_6, Science **346**, 1208 (2014).

[20] B. S. Tan, Y. T. Hsu, B. Zeng, M. C. Hatnean, N. Harrison, Z. Zhu, M. Hartstein, M. Kiourlappou, A. Srivastava, M. D. Johannes *et al.*, Unconventional Fermi surface in an insulating state, Science **349**, 287 (2015).

[21] Z. Xiang, B. Lawson, T. Asaba, C. Tinsman, L. Chen, C. Shang, X. H. Chen, and L. Li, Bulk Rotational Symmetry Breaking in Kondo Insulator SmB_6, Phys. Rev. X **7**, 031054 (2017).

[22] S. M. Thomas, X. X. Ding, F. Ronning, V. Zapf, J. D. Thompson, Z. Fisk, J. Xia, and P. F. S. Rosa, Quantum Oscillations in Flux-Grown SmB_6 with Embedded Aluminum, Phys. Rev. Lett. **122**, 166401 (2019).

[23] J. Denlinger, J. Allen, J.-S. Kang, K. Sun, J.-W. Kim, J. Shim, B. Min, D.-J. Kim, and Z. Fisk, Temperature dependence of linked gap and surface state evolution in the mixed valent topological insulator SmB_6, arXiv:1312.6637.

[24] E. Frantzeskakis, N. de Jong, B. Zwartsenberg, Y. K. Huang, Y. Pan, X. Zhang, J. X. Zhang, F. X. Zhang, L. H. Bao, O. Tegus *et al.*, Kondo Hybridization and the Origin of Metallic States at the (001) Surface of SmB_6, Phys. Rev. X **3**, 041024 (2013).

[25] J. Jiang, S. Li, T. Zhang, Z. Sun, F. Chen, Z. R. Ye, M. Xu, Q. Q. Ge, S. Y. Tan, X. H. Niu *et al.*, Observation of possible topological in-gap surface states in the Kondo insulator SmB_6 by photoemission, Nat. Commun. **4**, 3010 (2013).

[26] C. H. Min, P. Lutz, S. Fiedler, B. Y. Kang, B. K. Cho, H. D. Kim, H. Bentmann, and F. Reinert, Importance of Charge Fluctuations for the Topological Phase in SmB_6, Phys. Rev. Lett. **112**, 226402 (2014).

[27] H. Miyazaki, T. Hajiri, T. Ito, S. Kunii, and S.-i. Kimura, Momentum-dependent hybridization gap and dispersive in-gap state of the Kondo semiconductor SmB_6, Phys. Rev. B **86**, 075105 (2012).

[28] M. Neupane, N. Alidoust, S. Y. Xu, T. Kondo, Y. Ishida, D. J. Kim, C. Liu, I. Belopolski, Y. J. Jo, T. R. Chang *et al.*, Surface electronic structure of the topological Kondo-insulator candidate correlated electron system SmB_6, Nat. Commun. **4**, 2991 (2013).

[29] N. Xu, P. K. Biswas, J. H. Dil, R. S. Dhaka, G. Landolt, S. Muff, C. E. Matt, X. Shi, N. C. Plumb, M. Radovic *et al.*, Direct observation of the spin texture in SmB_6 as evidence of the topological Kondo insulator, Nat. Commun. **5**, 4566 (2014).

[30] M. M. Yee, Y. He, A. Soumyanarayanan, D.-J. Kim, Z. Fisk, and J. E. Hoffman, Imaging the Kondo insulating gap on SmB_6, arXiv:1308.1085.

[31] S. Rossler, T. H. Jang, D. J. Kim, L. H. Tjeng, Z. Fisk, F. Steglich, and S. Wirth, Hybridization gap and Fano resonance in SmB_6, Proc. Natl. Acad. Sci. U.S.A. **111**, 4798 (2014).

[32] W. Ruan, C. Ye, M. H. Guo, F. Chen, X. H. Chen, G. M. Zhang, and Y. Y. Wang, Emergence of a Coherent In-Gap State in the SmB_6 Kondo Insulator Revealed by Scanning Tunneling Spectroscopy, Phys. Rev. Lett. **112**, 136401 (2014).

[33] W. K. Park, L. N. Sun, A. Noddings, D. J. Kim, Z. Fisk, and L. H. Greene, Topological surface states interacting with bulk excitations in the Kondo insulator SmB_6 revealed via planar tunneling spectroscopy, Proc. Natl. Acad. Sci. U.S.A. **113**, 6599 (2016).

[34] L. Sun, D. J. Kim, Z. Fisk, and W. K. Park, Planar tunneling spectroscopy of the topological Kondo insulator SmB_6, Phys. Rev. B **95**, 195129 (2017).

[35] X. H. Zhang, N. P. Butch, P. Syers, S. Ziemak, R. L. Greene, and J. Paglione, Hybridization, Inter-Ion Correlation, and Surface States in the Kondo Insulator SmB_6, Phys. Rev. X **3**, 011011 (2013).

[36] Y. Sato, *Quantum Oscillations and Charge-Neutral Fermions in Topological Kondo Insulator* YbB_{12} (Springer, Singapore, 2021).

[37] F. Lu, J. Z. Zhao, H. M. Weng, Z. Fang, and X. Dai, Correlated Topological Insulators with Mixed Valence, Phys. Rev. Lett. **110**, 096401 (2013).

[38] V. Alexandrov, M. Dzero, and P. Coleman, Cubic Topological Kondo Insulators, Phys. Rev. Lett. **111**, 226403 (2013).

[39] T. Takimoto, SmB_6: A promising candidate for a topological insulator, J. Phys. Soc. Jpn. **80**, 123710 (2011).

[40] W. T. Fuhrman, J. Leiner, P. Nikolic, G. E. Granroth, M. B. Stone, M. D. Lumsden, L. DeBeer-Schmitt, P. A. Alekseev, J. M. Mignot, S. M. Koohpayeh *et al.*, Interaction Driven Subgap Spin Exciton in the Kondo Insulator SmB_6, Phys. Rev. Lett. **114**, 036401 (2015).

[41] G. A. Kapilevich, P. S. Riseborough, A. X. Gray, M. Gulacsi, T. Durakiewicz, and J. L. Smith, Incomplete protection of the surface Weyl cones of the Kondo insulator SmB_6: Spin exciton scattering, Phys. Rev. B **92**, 085133 (2015).

[42] A. Arab, A. X. Gray, S. Nemsak, D. V. Evtushinsky, C. M. Schneider, D. J. Kim, Z. Fisk, P. F. S. Rosa, T. Durakiewicz, and P. S. Riseborough, Effects of spin excitons on the surface states of SmB_6: A photoemission study, Phys. Rev. B **94**, 235125 (2016).

[43] J. Kim, C. Jang, X. F. Wang, J. Paglione, S. Hong, J. Lee, H. Choi, and D. Kim, Electrical detection of the surface spin polarization of the candidate topological Kondo insulator SmB_6, Phys. Rev. B **99**, 245148 (2019).

[44] L. Kong, Y. Zhou, S. Liu, Z. Lin, L. Zhang, F. Lin, D. Tang, H.-C. Wu, J. Liu, H.-Z. Lu *et al.*, Spin-polarized surface state transport in a topological Kondo insulator SmB_6 nanowire, Phys. Rev. B **95**, 235410 (2017).

[45] P. Hlawenka, K. Siemensmeyer, E. Weschke, A. Varykhalov, J. Sanchez-Barriga, N. Y. Shitsevalova, A. V. Dukhnenko, V. B. Filipov, S. Gabani, K. Flachbart *et al.*, Samarium hexaboride is a trivial surface conductor, Nat. Commun. **9**, 517 (2018).

[46] G. Akopov, M. T. Yeung, and R. B. Kaner, Rediscovering the crystal chemistry of borides, Adv. Mater. **29**, 1604506 (2017).

[47] H. M. Weng, J. Z. Zhao, Z. J. Wang, Z. Fang, and X. Dai, Topological Crystalline Kondo Insulator in Mixed Valence Yterbium Borides, Phys. Rev. Lett. **112**, 016403 (2014).

[48] L. A. Fu, Topological Crystalline Insulators, Phys. Rev. Lett. **106**, 106802 (2011).

[49] T. H. Hsieh, H. Lin, J. W. Liu, W. H. Duan, A. Bansil, and L. Fu, Topological crystalline insulators in the SnTe material class, Nat. Commun. **3**, 982 (2012).

[50] Y. Sato, Z. Xiang, Y. Kasahara, S. Kasahara, L. Chen, C. Tinsman, F. Iga, J. Singleton, N. L. Nair, N. Maksimovic *et al.*, Topological surface conduction in Kondo insulator YbB_{12}, J. Phys. D: Appl. Phys. **54**, 404002 (2021).

[51] Y. Sato, Z. Xiang, Y. Kasahara, T. Taniguchi, S. Kasahara, L. Chen, T. Asaba, C. Tinsman, H. Murayama, O. Tanaka *et al.*, Unconventional thermal metallic state of charge-neutral fermions in an insulator, Nat. Phys. **15**, 954 (2019).

[52] H. Okamura, T. Michizawa, T. Nanba, S. Kimura, F. Iga, and T. Takabatake, Indirect and direct energy gaps in Kondo semiconductor YbB_{12}, J. Phys. Soc. Jpn. **74**, 1954 (2005).

[53] T. Susaki, A. Sekiyama, K. Kobayashi, T. Mizokawa, A. Fujimori, M. Tsunekawa, T. Muro, T. Matsushita, S. Suga, H. Ishii *et al.*, Low-energy Electronic Structure of the Kondo Insulator YbB_{12}, Phys. Rev. Lett. **77**, 4269 (1996).

[54] M. Okawa, Y. Ishida, M. Takahashi, T. Shimada, F. Iga, T. Takabatake, T. Saitoh, and S. Shin, Hybridization gap formation in the Kondo insulator YbB_{12} observed using time-resolved photoemission spectroscopy, Phys. Rev. B **92**, 161108(R) (2015).

[55] J. M. Mignot, P. A. Alekseev, K. S. Nemkovski, L. P. Regnault, F. Iga, and T. Takabatake, Evidence for Short-Range Antiferromagnetic Fluctuations in Kondo-Insulating YbB_{12}, Phys. Rev. Lett. **94**, 247204 (2005).

[56] J. M. Mignot, P. A. Alekseev, K. S. Nemkovski, E. V. Nefeodova, A. Rybina, L. P. Regnault, N. Y. Shitsevalova, F. Iga, and T. Takabatake, Neutron scattering study of spin and lattice dynamics in YbB_{12}, Physica B **383**, 16 (2006).

[57] F. Iga, K. Suga, K. Takeda, S. Michimura, K. Murakami, T. Takabatake, and K. Kindo, Anisotropic magnetoresistance and collapse of the energy gap in $Yb_{1-x}Lu_xB_{12}$, J. Phys. Conf. Ser. **200**, 012064 (2010).

[58] T. T. Terashima, A. Ikeda, Y. H. Matsuda, A. Kondo, K. Kindo, and F. Iga, Magnetization process of the Kondo insulator YbB_{12} in ultrahigh magnetic fields, J. Phys. Soc. Jpn. **86**, 054710 (2017).

[59] T. T. Terashima, Y. H. Matsuda, Y. Kohama, A. Ikeda, A. Kondo, K. Kindo, and F. Iga, Magnetic-Field-Induced Kondo Metal Realized in YbB_{12}, Phys. Rev. Lett. **120**, 257206 (2018).

[60] H. Liu, M. Hartstein, G. J. Wallace, A. J. Davies, M. C. Hatnean, M. D. Johannes, N. Shitsevalova, G. Balakrishnan, and S. E. Sebastian, Fermi surfaces in Kondo insulators, J. Phys.: Condens. Matter **30**, 16LT01 (2018).

[61] Z. J. Xiang, L. Chen, K. W. Chen, C. Tinsman, Y. Sato, T. Asaba, H. E. Lu, Y. Kasahara, M. Jaime, F. Balakirev *et al.*, Unusual high-field metal in a Kondo insulator, Nat. Phys. **17**, 788 (2021).

[62] H. Liu, A. J. Hickey, M. Hartstein, A. J. Davies, A. G. Eaton, T. Elvin, E. Polyakov, T. H. Vu, V. Wichitwechkarn, T. Forster *et al.*, f-electron hybridised Fermi surface in magnetic field-induced metallic YbB_{12}, npj Quantum Mater. **7**, 12 (2022).

[63] Z. Xiang, Y. Kasahara, T. Asaba, B. Lawson, C. Tinsman, L. Chen, K. Sugimoto, S. Kawaguchi, Y. Sato, G. Li *et al.*, Quantum oscillations of electrical resistivity in an insulator, Science **362**, 65 (2018).

[64] Z. Xiang, K.-W. Chen, L. Chen, T. Asaba, Y. Sato, N. Zhang, D. Zhang, Y. Kasahara, F. Iga, W. A. Coniglo *et al.*, Hall Anomaly, Quantum Oscillations and Possible Lifshitz Transitions in Kondo Insulator YbB_{12}: Evidence for Unconventional Charge Transport, Phys. Rev. X **12**, 021050 (2022).

[65] K. Hagiwara, Y. Ohtsubo, M. Matsunami, S. Ideta, K. Tanaka, H. Miyazaki, J. E. Rault, P. Le Fevre, F. Bertran, A. Taleb-Ibrahimi *et al.*, Surface Kondo effect and non-trivial metallic state of the Kondo insulator YbB_{12}, Nat. Commun. **7**, 12690 (2016).

[66] W. A. Phelan, S. M. Koohpayeh, P. Cottingham, J. A. Tutmaher, J. C. Leiner, M. D. Lumsden, C. M. Lavelle, X. P. Wang, C. Hoffmann, M. A. Siegler *et al.*, On the chemistry and physical properties of flux and floating zone grown SmB_6 single crystals, Sci. Rep. **6**, 20860 (2016).

[67] See Supplemental Material at http://link.aps.org/supplemental/10.1103/PhysRevB.107.165132 for surface topographic images from atomic force microscopy, comparison of the normalized

resistance between YbB_{12} and SmB_6 crystals, and additional conductance spectra.

[68] J. A. Sittler and W. K. Park, Self-oxidation-formed boron oxide as a tunnel barrier in SmB_6 junctions, J. Alloy Compd. **874**, 159841 (2021).

[69] W. K. Park, J. A. Sittler, L. H. Greene, W. T. Fuhrman, J. R. Chamorro, S. M. Koohpayeh, W. A. Phelan, and T. M. McQueen, Topological nature of the Kondo insulator SmB_6 and its sensitiveness to Sm vacancy, Phys. Rev. B **103**, 155125 (2021).

[70] W. F. Brinkman, R. C. Dynes, and J. M. Rowell, Tunneling conductance of asymmetrical barriers, J. Appl. Phys. **41**, 1915 (1970).

[71] https://doi.org/10.34863/r874-fw50.